Electronic and magnetic properties of ultrathin rhodium nanowires

2003 J. Phys.: Condens. Matter 15 2327

(http://iopscience.iop.org/0953-8984/15/14/308)

INSTITUTE OF PHYSICS PUBLISHING JOURNAL OF PHYSICS: CONDENSED MATTER

J. Phys.: Condens. Matter **15** (2003) 2327–2334 PII: S0953-8984(03)53599-8

Electronic and magnetic properties of ultrathin rhodium nanowires

Baolin Wang[1,2,5], Guanghou Wang[1], Yun Ren[1], Houqian Sun[3], Xiaoshuang Chen[4] and Jijun Zhao[5]

[1] National Laboratory of Solid State Microstructures and Department of Physics, Nanjing University, Nanjing 210093, People's Republic of China
[2] Department of Physics, Huaiyin Teachers College, Jiangsu 223001, People's Republic of China
[3] Department of Physics, Yancheng Institute of Technology, Jiangsu 224502, People's Republic of China
[4] National Laboratory for Infrared Physics, Shanghai Institute of Technical Physics, Chinese Academy of Sciences, Shanghai 224502, People's Republic of China
[5] Department of Physics and Astronomy, University of North Carolina at Chapel Hill, Chapel Hill, NC 27599, USA

E-mail: ghwang@nju.edu.cn and jzhao@wsu.edu

Received 18 September 2002
Published 31 March 2003
Online at stacks.iop.org/JPhysCM/15/2327

Abstract

The structures of ultrathin rhodium nanowires are studied using empirical molecular dynamics simulations with a genetic algorithm. Helical multishell cylindrical and pentagonal packing structures are found. The electronic and magnetic properties of the rhodium nanowires are calculated using an spd tight-binding Hamiltonian in the unrestricted Hartree–Fock approximation. The average magnetic moment and electronic density of states are obtained. Our results indicate that the electronic and magnetic properties of the rhodium nanowires depend not only on the size of the wire but also on the atomic structure. In particular, centred pentagonal and hexagonal structures can be unusually ferromagnetic.

1. Introduction

In recent years, ultrathin metallic nanowires have attracted much attention for both fundamental and technological reasons. Experimentally, ultrathin metallic nanowires have been manufactured using different techniques [1–6]. In particular, Takayanagi's group has successfully fabricated stable gold and platinum wires with diameters from about 0.5 to 3 nm of sufficient length [4–6] suspended in a vacuum between two stands. Novel helical multishell structures are found for these free-standing ultrathin nanowires [5, 6]. On the theoretical side, the melting behaviour, noncrystalline structure and electronic properties of ultra-thin free-standing lead, aluminium and silver nanowires have been studied by Tosatti's group [7–10]. By using molecular dynamics-based genetic algorithm simulations, our group

has systematically studied the structural, vibrational, melting and electronic properties of gold, titanium and zirconium nanowires [11–14]. However, our current knowledge about metallic nanowires is still quite limited. In particular, there are almost no theoretical studies on the electronic and magnetic properties of ultrathin transition metal nanowires.

From an early experiment [15] and some theoretical works [16–20] it is well known that small rhodium clusters may possess a permanent magnetic moment, although bulk rhodium is a nonmagnetic solid. The average magnetic moment/atom oscillates with cluster sizes and converges to zero when the cluster is large enough (∼100 atoms). This phenomenon can be intuitively understood by the decrease of coordination number and narrowing of 4d bands [16]. Similarly, the possible existence of ferromagnetism in thin films and surfaces of rhodium metal has also been investigated both theoretically [21–24] and experimentally [25, 26]. Recent experiments by Goldoni *et al* [26] have provided clear evidence of magnetic ordering at the Rh(100) surface. Therefore, it is interesting to explore if a one-dimensional ultra-thin rhodium nanowire could be ferromagnetic, as is the case for zero-dimensional clusters and two-dimensional slabs or surfaces. In this paper we use an empirical genetic algorithm to determine the optimal structure of rhodium nanowires. The electronic and magnetic properties of these nanowires are then calculated within a spin-polarized tight-binding Hamiltonian.

2. Theoretical method

The total cohesive energy of a transition metal system can be described by a Gupta-like model potential [27, 28]:

$$E = \sum_i \left\{ \sum_{j\neq i} B \exp\left[-p\left(\frac{r_{ij}}{r_0} - 1 \right) \right] - \left(\sum_{j\neq i} A^2 \exp\left[-2q\left(\frac{r_{ij}}{r_0} - 1 \right) \right] \right)^{1/2} \right\} \tag{1}$$

where the two terms represent the electronic band energy and the Born–Mayer repulsive interaction respectively. r_{ij} stands for the distance between sites i and j. r_0 is the equilibrium distance in the bulk solid. A, B, p, q are adjustable parameters that are fitted to reproduce the equilibrium interatomic distance and cohesive energy of both bulk solid rhodium and the Rh_2 dimer [29]. Our previous fitted parameter set, $A = 1.47$ eV, $B = 0.1045$ eV, $p = 10.6$, $q = 2.61$ [20], is used in this work. The Gupta-like potential has been widely used in describing the structural and dynamical properties of transition metal nanostructures. For rhodium clusters, our previous work shows that the geometric parameters like bond length agree reasonably with first-principles spin-polarized calculations (see tables 2 and 3 in [20]).

With the interatomic potential described in equation (1), fully geometric optimization of rhodium nanowires with diameters from 0.48 to 1.35 nm are performed by using a genetic algorithm incorporated into molecular dynamics simulations [30]. The length of the supercell along the direction of the wire axis is chosen to be between 1.0 and 1.4 nm, as a reasonable compromise to attain helical structures in one-dimensional nanowires. Details of the genetic algorithm simulation have been described in our previous works [11–14].

The electronic and magnetic properties of rhodium nanowires were investigated using a parametrized tight-binding Hamiltonian in the Hartree–Fock approximation [31–34]. The same method has been successfully applied to rhodium clusters [20] and the results are in good agreement with *ab initio* calculations. Within a local orbital basic set, the Hamiltonian is written as

$$H = \sum_{i,\alpha,\sigma} \varepsilon_{i\alpha\sigma} \hat{n}_{i\alpha\sigma} + \sum_{i\neq j;\alpha,\beta,\sigma} t_{ij}^{\alpha\beta} \hat{C}_{i\alpha\sigma}^{+} \hat{C}_{j\beta\sigma}. \tag{2}$$

Table 1. Tight-binding parameters (in units of eV) for Rh used in this work.

$\varepsilon_s = 1.87$	$t_{ss\sigma} = -0.97$
$\varepsilon_p = 5.92$	$t_{sp\sigma} = 1.20$
$\varepsilon_d(\mathrm{T_{2g}}) = -2.96$	$t_{pp\sigma} = 1.50$
$\varepsilon_d(\mathrm{E_g}) = -3.17$	$t_{pp\pi} = -0.19$
	$t_{sd\sigma} = -0.97$
$U_{ss} = 0.95$	$t_{pd\sigma} = -1.22$
$U_{sd} = 1.05$	$t_{pd\pi} = 0.29$
$U_{dd} = 2.636$	$t_{dd\sigma} = -1.04$
	$t_{dd\pi} = 0.42$
$J_{dd} = 0.60$	$t_{dd\delta} = -0.02$

Here $\hat{C}^{+}_{i\alpha\sigma}$ is the operator for the creation of an election with spin σ and orbital state α ($\alpha = \mathrm{s}, \mathrm{p}_x, \mathrm{p}_y, \mathrm{p}_z, \mathrm{d}_{xy}, \mathrm{d}_{yz}, \mathrm{d}_{zx}, \mathrm{d}_{x^2-y^2}, \mathrm{d}_{3z^2-r^2}$) at the atomic site i, $\hat{C}_{i\alpha\sigma}$ is the annihilation operator and $\hat{n}_{i\alpha\sigma}$ refers to the number operator of an electron. The $t^{\alpha\beta}_{ij}$ are the hopping elements of the Hamiltonian. The $\varepsilon_{i\alpha\sigma}$ denotes the on-site Hartree–Fock energy and is given by

$$\varepsilon_{i\alpha\sigma} = \varepsilon^0_{i\alpha} + \sum_{\beta} U_{\alpha\beta}\Delta\nu_{i\beta} - \sigma\sum_{\beta}\frac{J_{\alpha\beta}}{2}\mu_{i\beta} + \Delta\varepsilon^{Mad}_{i\alpha} + Z_i\Omega_\alpha. \tag{3}$$

Here $\varepsilon^0_{i\alpha}$ refers to the orbital energy levels in the paramagnetic solutions of the bulk, $\Delta\nu_{i\beta} = \nu_{i\beta} - \nu^0_{i\beta}$, $\nu_{i\beta} = \langle\hat{n}_{i\beta\uparrow}\rangle + \langle\hat{n}_{i\beta\downarrow}\rangle$ is the average electronic occupation at orbital β of atomic site i and $\nu^0_{i\beta}$ is the average electronic occupation of the paramagnetic solution of the bulk. $\mu_{i\beta}$ is the local magnetic moment at the orbital β of site i. $J_{\alpha\beta}$ and $U_{\alpha\beta}$ are the exchange and the direct integrals, respectively. Andersen's LMTO-ASA parameters [35] for the tight-binding hopping integrals are used as in [33]. All the other parameters such as $\varepsilon^0_{i\alpha}$ $J_{\alpha\beta}$ and $U_{\alpha\beta}$ are taken from [33]. All these parameters are given in table 1.

The Madelung term in equation (3) consists of a sum in real space of electrostatic potentials over all sites:

$$\Delta\varepsilon^{Mad}_{i\alpha} = \sum_{j\neq i}\sum_{\beta} V_{i\alpha j\beta}, \tag{4}$$

with

$$V_{i\alpha j\beta} = \frac{U_{\alpha\beta}\Delta\nu_{j\beta}}{1 + \frac{U_{\alpha\beta}R_{ij}}{e^2}}. \tag{5}$$

The last term $Z_i\Omega_\alpha$ in equation (3) takes into account the energy-level corrections due to nonorthogonality effects, and the crystal-field potential of the neighbouring atoms [32], which are approximately proportional to the local coordination number Z_i. The orbital-dependent constant Ω_α is obtained from the difference between the bare energy levels (i.e. excluding Coulomb shifts) of the isolated atom and the bulk as $\Omega_s = 0.18$ eV, $\Omega_p = 0.27$ eV, $\Omega_d = -0.15$ eV [20, 32].

The number of electrons $n(i)$ and the local magnetic moments $\mu(i)$ at site i, are given by

$$n(i) = \sum_{\alpha}\langle\hat{n}_{i\alpha\uparrow}\rangle + \sum_{\alpha}\langle\hat{n}_{i\alpha\downarrow}\rangle \tag{6}$$

and

$$\mu(i) = \sum_{\alpha}\langle\hat{n}_{i\alpha\uparrow}\rangle - \sum_{\alpha}\langle\hat{n}_{i\alpha\downarrow}\rangle, \tag{7}$$

$$\langle\hat{n}_{i\alpha\sigma}\rangle = \int_{-\infty}^{\varepsilon_f}\rho_{i\alpha\sigma}(\varepsilon)\,\mathrm{d}\varepsilon. \tag{8}$$

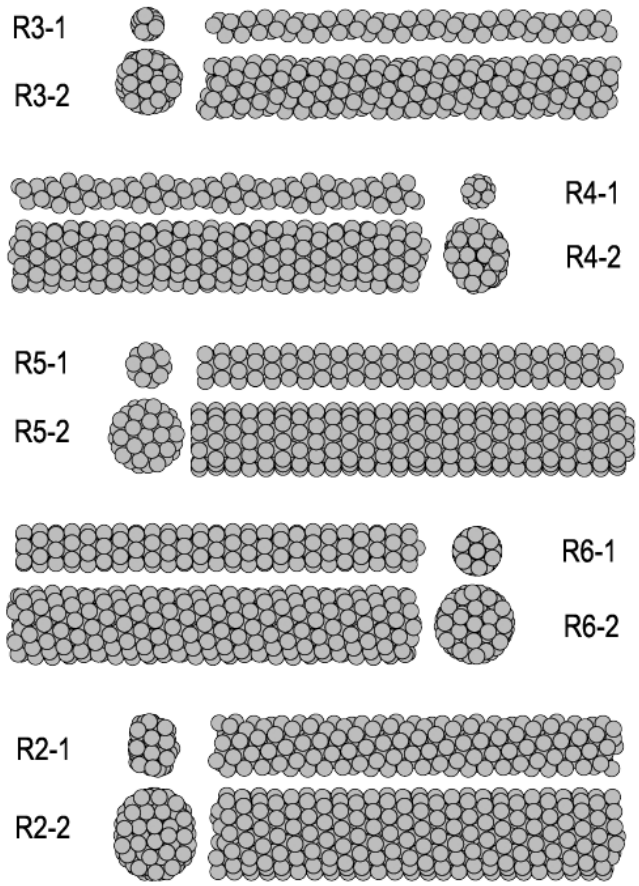

Figure 1. Structures of Rh nanowires with diameters from 0.48 to 1.35 nm in growing patterns of trigonal (R3-1, R3-2), tetragonal (R4-1, R4-2), centred pentagonal (R5-1, R5-2), centred hexagonal (R6-1, R6-2) packing, and double-strand core (R2-1, R2-2) are presented.

During the calculations, the energy of the highest occupied state (Fermi energy) ε_f is determined from the global charge neutrality condition. The local density of states (DOS) with spin σ at orbital α of site i is obtained by calculating the local Green function $G_{i\alpha\sigma,i\alpha\sigma}$ by means of the recursion method [36].

$$\rho_{i\alpha\sigma} = -\frac{1}{\pi}\mathrm{Im}\, G_{i\alpha\sigma,i\alpha\sigma}(\varepsilon). \tag{9}$$

Thus, the local magnetic moments and the average magnetic moments of rhodium nanowires are determined at the end of a self-consistent procedure.

3. Structures of rhodium nanowires

Figure 1 shows some typical rhodium nanowire morphologies obtained from genetic algorithm optimization. These structures are multishell cylinders composed of coaxial cylindrical tubes (or shells). Each shell consists of helical rows of atom wound up helically side-by-side. The pitch of the helix is different between the outer and inner shells. The lateral surface of the multishell nanowires is formed by nearly triangular network structures. Such helical multishell structures have been theoretically predicted for Al, Pb [8], Au [11], Ti [12] and

Zr [13], and observed in Au and Pt nanowires in recent experiments [5, 6]. The thinnest wire R3-1 (wire diameter $D = 0.48$ nm) in figure 1 has a three-strand helical structure. Wire R3-2 ($D = 0.97$ nm) is formed by double-walled shells, i.e. the outer shell contains nine strands and the inner shell has three strands. Wire R4-1 ($D = 0.55$ nm) has four strands, while R4-2 ($D = 1.03$ nm) is composed of nine strands in the outer shell and four strands in the inner shell. R5-1 ($D = 0.69$ nm) and R5-2 ($D = 1.13$ nm) wires in figure 1 represent growth patterns with two-shell and three-shell centred pentagonal structures. The innermost shell of these wires consists of a single strand of atoms. Such structures can be related to the deformed icosahedral packing found in rhodium clusters [17, 20, 22]. The wires R6-1 ($D = 0.76$ nm) and R6-2 ($D = 1.19$ nm) in figure 1 show a centred hexagonal growth patterns with two and three outer atomic shells. The centre of nanowires R2-1 ($D = 0.86$ nm) and R2-2 ($D = 1.35$ nm) consists of nearly parallel double atomic rows. The surrounding shells are made up of 8 and 13 identical strands respectively. Systematic illustrations of various multishell growth sequences of the metal nanowires can be found in our previous work on Zr nanowires [13].

For each nanowire, we may divide the n atoms in the supercell into several groups. The atomic sites belonging to each group are all geometrically equivalent. Due to the significant structural distortion, no geometrically equivalent sites could be defined in R3-1, R3-2, R4-1, R4-2, R2-1 and R2-2 wires. Thus, in these wires, each atom stands for one nonequivalent group. There are two nonequivalent sites (i.e. centred single row and outer shell) in R5-1 and R6-1 wires, seven in R5-2 and twelve in R6-2.

4. Electronic states and magnetic properties of rhodium nanowires

Based on the optimized geometries, we calculate the average magnetic moment of ten rhodium nanowires in figure 1, starting from the atomic configuration $4d^8\,5s^1\,5p^0$. The theoretical results are summarized in table 2 along with the diameter (D), the average coordination number ($\bar{Z}$) and average bond length ($\bar{r}$) of the rhodium nanowires. Our results show that all the ultrathin rhodium nanowires studied are magnetic. The moments of the nanowires decrease rapidly with increasing wire diameter. For rhodium nanowires this is indirectly supported by experiments on rhodium clusters. The magnetic moments for Rh_n clusters with $n > 60$–90 are less than 0.1 μ_b/atom [15].

Rather high magnetic moments of 0.595 and 0.766 μ_b/atom are found for R5-1 and R6-1 wires respectively. It is worth noting that the structures of R5-1 and R6-1 wires are comparable to Rh_{19} and Rh_{15} clusters respectively with relatively higher symmetries (D_{5h} and D_{6h}) [20]. The enhanced magnetic moments in R5-1 and R6-1 wires can be understood by the same arguments used to explain the larger magnetic moments in Rh_{19} and Rh_{15} clusters [20]. In these clusters, high degeneracy in the electronic DOS leads to larger magnetization. The calculated average moments/atom for R5-2 and R6-2 wires are 0.157 and 0.237 μ_b.

For the R3-1 and R4-1 wires having helical packing without centred atom chains, the lower symmetry leads to smaller magnetic moments. Accordingly, R3-2 and R4-2 wires have very low magnetic moment of 0.101 and 0.088 μ_b/atom. In the case of a free-standing rhodium slab, the monolayer and bilayer are found to be magnetic and nonmagnetic respectively [33]. The calculated average magnetic moment of the double-chain core R2-1 wire is 0.262 μ_b/atom, larger than that of R3-1 and R4-1 wires. The magnetic moment of the thickest wire, R2-2, is almost zero. Compared with the R3-2 and R4-2 wires without centred atomic rows, the centre-atom core wires (i.e. the centred pentagonal and hexagonal wires) are more favourable to larger magnetization due to their relatively higher symmetries, even for the thicker R5-2 and R6-2 wires. The straight centre-atom chains of the rhodium nanowires have a very peculiar behaviour, similar to the centre atom in Rh clusters [20].

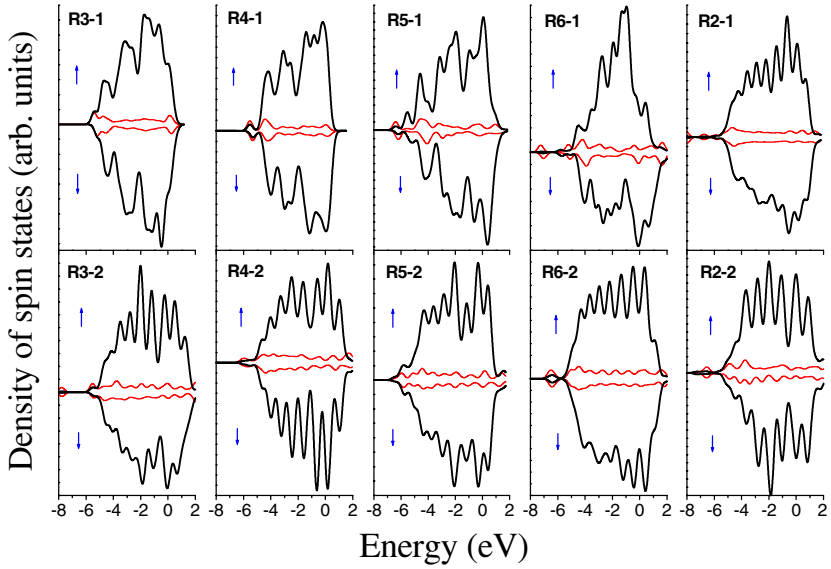

Figure 2. Calculated density of electronic states for majority and minority spins of sp (thinner curves) and d electron (thicker curves) of R3-1, R3-2, R4-1, R4-2, R5-1, R5-2, R6-1, R6-2, R2-1 and R2-2 nanowires. The Fermi energy is shifted to the origin. 0.2 eV Gaussian broadening is used.

(This figure is in colour only in the electronic version)

Table 2. The diameter D, average bond length $\bar{r}$, average coordination number $\bar{Z}$ and calculated average magnetic moments/atom μ_n for rhodium nanowires.

Nanowires	R3-1	R3-2	R4-1	R4-2	R5-1	R5-2	R6-1	R6-2	R2-1	R2-2
D (nm)	0.48	0.97	0.55	1.03	0.69	1.13	0.76	1.19	0.86	1.35
$\bar{r}$ (Å)	2.61	2.64	2.67	2.65	2.68	2.67	2.68	2.64	2.65	2.66
$\bar{Z}$	6.00	8.89	7.00	9.01	8.67	9.81	8.86	9.27	8.50	9.47
μ_n (μ_b)	0.187	0.101	0.251	0.088	0.595	0.157	0.766	0.237	0.262	0.018

Figure 2 shows the spin-polarized DOS for sp and d electrons in the rhodium nanowires. From figure 2 it can be seen that the electronic states near the Fermi level are dominated by d character. For electronic states well below and above, the sp contributions become important. In particular, large spd mixings are found near the edges of the d band. The density of spin states of the thinner wires R3-1, R4-1, R5-1, R6-1 and R2-1 in figure 2 are very close to those of Rh_n clusters given by LSD calculations in [17] and the tight-binding DOS for the Rh(001) monolayer [37]. The densities of spin states of the thicker wires R3-2, R4-2, R5-2, R6-2 and R2-2 are similar to those of Rh monolayers grown epitaxially on Au (001) [37] and Ag (001) [38]. The exchange splitting found for R5-1 and R6-1 wires is larger than that for the other wires, in agreement with the calculated magnetic moments for the nanowires (see table 2).

As compared with the bulk DOS [22, 24], the main feature of the DOS for nanowires is the narrowing of the bandwidth. The electronic band gradually broadens as the wires become thicker. The narrowing of bandwidth due to the reduced coordination number and large surface ratio is a well known fact for transition metal clusters [16]. The DOS of the thinner nanowire

(R3-1, R4-1) shows some features similar to Rh clusters. In particular, the DOS of R5-1 is very close to those of Rh_{13} and Rh_{19} clusters [17, 22], which can be attributed to their common pentagonal symmetry. For the thicker wires, the DOSs are close to those of the Rh bare surface and slab surface [21–24]. There are still certain deviations from the bulk DOS even in thickest nanowires studied (see the three dominant peaks). These differences are due to the structural difference between the helical multishell nanowire and the fcc solid. As the wire diameter keeps increasing, the nanowire DOS should gradually approach that of the bulk, which may be accompanied by a transition to an fcc-like structure [11].

In summary, we have performed geometric optimization on ultrathin rhodium nanowires by using empirical genetic algorithm simulations. Helical multishell cylindrical structures with different growth patterns, such as trigonal, tetragonal, centred pentagonal and centred hexagonal packing, are obtained for Rh wires. The electronic and magnetic properties of rhodium nanowires are investigated with an spd tight-binding Hamiltonian. All the nanowires studied are ferromagnetic. The magnetic properties of rhodium nanowires are related not only to their size but also to their structure. The centred pentagonal and hexagonal wires have particularly high magnetic moments. The electronic and magnetic behaviour of ultrathin nanowires is similar to that of other low-dimensional systems such as Rh clusters, slabs and surfaces. It is worth noting that both the Gupta-like potential and the tight-binding model Hamiltonian can only quantitatively describe the structural and magnetic properties of rhodium nanowires. However, the prediction of the strong ferromagnetism in some nanowires is robust and should not depend on the theoretical methods. We expect future experiments and *ab initio* calculations on rhodium nanowires to validate our arguments.

Acknowledgments

B L Wang, Y Ren and G H Wang would like to thank the National Nature Science Foundation of China for financial support (nos 90206033, 10023001). J J Zhao acknowledges support from the University Research Council of the University of North Carolina at Chapel Hill.

References

[1] Lisiecki L, Filankembo A, Sack-Kongehl H, Weiss K, Pileni M P and Urban J 2000 *Phys. Rev.* B **61** 4968
[2] Yun W S *et al* 2000 *J. Vac. Sci. Technol.* A **18** 1329
[3] Lin J L, Petrovykh D Y, Kirakosian A, Rauscher H, Himpse F J and Dowben P A 2001 *Appl. Phys. Lett.* **78** 829
[4] Kondo Y and Takayanagi K 1997 *Phys. Rev. Lett.* **79** 3455
Ohnishim H, Kondo Y and Takayanagi K 1998 *Nature* **395** 780
[5] Kondo K and Takayanagi K 2000 *Science* **289** 606
[6] Oshima Y, Koirumi H, Mouri K, Hirayama H, Takayanagi K and Kondo Y 2002 *Phys. Rev.* B **65** 121401
[7] Gulseren O, Ercolessi F and Tosatti E 1995 *Phys. Rev.* B **51** 7377
[8] Gulseren O, Ercolessi F and Tosatti E 1998 *Phys. Rev. Lett.* **80** 3775
[9] Di Tolla F, Dal Corso A, Torres J A and Tosatti E 2000 *Surf. Sci.* **456** 947
[10] Tosatti E, Prestipino S, Kostlmeier S, Dal Corso A and Tolla F D 2001 *Science* **291** 288
[11] Wang B L, Yin S Y, Wang G H, Buldum A and Zhao J J 2001 *Phys. Rev. Lett.* **86** 2043
[12] Wang B L, Yin S Y, Wang G H and Zhao J J 2001 *J. Phys.: Condens. Matter* **13** L403
[13] Wang B L, Zhao J J and Wang G H 2002 *Phys. Rev.* B **65** 235406
[14] Wang J L, Chen X S, Wang G H, Wang B L, Lu W and Zhao J J 2002 *Phys. Rev.* B **66** 085408
[15] Cox A J, Louderback J G and Bloomfield L A 1993 *Phys. Rev. Lett.* **71** 923
Cox A J, Louderback J G, Apsel S E and Bloomfield L A 1994 *Phys. Rev.* B **49** 12295
[16] Zhao J J, Chen X S, Sun Q, Liu F Q and Wang G H 1995 *Europhys. Lett.* **32** 113
[17] Jinlong Y, Toigo F and Kelin W 1994 *Phys. Rev.* B **50** 7915
Jinlong Y, Toigo F, Kelin W and Manhong Z 1994 *Phys. Rev.* B **50** 7173
[18] Li Z Q, Yu J Z, Ohno K and Kawazoe Y 1995 *J. Phys.: Condens. Matter* **7** 47

[19] Villasenor-Gonzălez P, Dorantes-Dăvila J, Dreyssĕ H and Pastor G M 1997 *Phys. Rev.* B **55** 15084
[20] Sun H Q, Ren Y, Luo Y H and Wang G H 2001 *Physica* B **293** 260
[21] Nayak S K, Weber S E, Jena P, Wildberger K, Zeller R, Dederichs P H, Stepanyuk V S and Hergert W 1997 *Phys. Rev.* B **56** 8849
[22] Barreteau C, Spanjaard D and Desjonqueres M C 1998 *Phys. Rev.* B **58** 9721
[23] Barreteau C, Gurado-Lopez R, Spanjaard D, Desjonqueres M C and Oles A M 2000 *Phys. Rev.* B **61** 7781
[24] Eichler A, Hafner J, Furthmuller J and Kresse G 1996 *Surf. Sci.* **346** 300
[25] Wu S C, Garrison K, Begley A M, Jona F and Johnson P D 1994 *Phys. Rev.* B **49** 14081
[26] Goldoni A, Baraldi A, Comelli G, Lizzit S and Paolucci G 1999 *Phys. Rev. Lett.* **82** 3156
Goldoni A, Baraldi A, Comelli G, Esch F, Larciprete R, Lizzit S and Paolucci G 2001 *Phys. Rev.* B **63** 035405
[27] Gupta R P 1981 *Phys. Rev.* B **23** 6265
[28] Cleri F and Rosato V 1993 *Phys. Rev.* B **48** 22
[29] Morse M D 1986 *Chem. Rev.* **86** 1049
[30] Luo Y H, Zhao J J, Qiu S T and Wang G H 1999 *Phys. Rev.* B **59** 14903
Li T X, Yin S Y, Ji Y L, Wang B L, Wang G H and Zhao J J 2000 *Phys. Lett.* A **267** 403
Zhao J J, Luo Y H and Wang G H 2001 *Eur. J. Phys.* D **14** 309
[31] Pastor G M, Dorantes-Dăvila J and Bennemann K H 1989 *Phys. Rev.* B **40** 7642
[32] Vega A, Dorantes-Dăvila J, Balbăs L C and Pastor G M 1993 *Phys. Rev.* B **47** 4742
[33] Fabricius G, liois A M, Weissmann M and Khan M A 1994 *Phys. Rev.* B **49** 2121
[34] Zhao J J, Chen X S, Sun Q, Liu F Q, Wang G H and Lain K D 1995 *Physica* B **215** 377
Chen X S, Zhao J J and Wang G H 1995 *Z. Phys.* D **35** 149
[35] Andersen O K, Jepsen O and Gloetzel D 1985 *Highlights of Condensed Matter Theory* ed F Bassani, F Fumi and M Tosi (Amsterdam: North-Holland)
[36] Haydock R, Heine V and Kelly M J 1975 *J. Phys. C: Solid State Phys.* **8** 2591
Heine V 1980 *Solid State Physics* vol 35 (New York: Academic)
[37] Zhu M J, Bylander D M and Kleinman L 1991 *Phys. Rev.* B **43** 4007
[38] Blugel S 1992 *Europhys. Lett.* **18** 257
Redinger J, Blugel S and Podloucky R 1995 *Phys. Rev.* B **51** 13852